www.nature.com/aps

Acta Pharmacologica Sinica

ARTICLE

Identification of nagilactone E as a protein synthesis inhibitor with anticancer activity

Le-le Zhang[1,2], Jing Guo[3], Xiao-ming Jiang[1], Xiu-ping Chen[1], Yi-tao Wang[1], Ao Li[4], Li-gen Lin[1], Hua Li[3] and Jin-jian Lu[1]

Norditerpenoids and dinorditerpenoids represent diterpenoids widely distributed in the genus *Podocarpus* with notable chemical structures and biological activities. We previously reported that nagilactone E (NLE), a dinorditerpenoid isolated from *Podocarpus nagi*, possessed anticancer effects against lung cancer cells in vitro. In this study we investigated the in vivo effect of NLE against lung cancer as well as the underlying mechanisms. We administered NLE (10 mg·kg^{-1}·d^{-1}, ip) to CB-17/SCID mice bearing human lung cancer cell line A549 xenograft for 3 weeks. We found that NLE administration significantly suppressed the tumor growth without obvious adverse effects. Thereafter, RNA sequencing (RNA-seq) analysis was performed to study the mechanisms of NLE. The effects of NLE on A549 cells have been illustrated by GO and pathway enrichment analyses. CMap dataset analysis supported NLE to be a potential protein synthesis inhibitor. The inhibitory effect of NLE on synthesis of total de novo protein was confirmed in Click-iT assay. Using the pcDNA3-RLUC-POLIRES-FLUC luciferase assay we further demonstrated that NLE inhibited both cap-dependent and cap-independent translation. Finally, molecular docking revealed the low-energy binding conformations of NLE and its potential target RIOK2. In conclusion, NLE is a protein synthesis inhibitor with anticancer activity.

Keywords: nagilactone E; diterpenoids; human lung cancer A549 cell line xenograft; RNA-seq; CMap; Click-iT; molecular docking; RIOK2; protein synthesis inhibitor

Acta Pharmacologica Sinica (2020) 41:698–705; https://doi.org/10.1038/s41401-019-0332-7

INTRODUCTION

Norditerpenoids and dinorditerpenoids are diterpenoids widely distributed in the genus *Podocarpus* with notable chemical structures [1, 2]. To date, a number of norditerpenoids and dinorditerpenoids have been identified and isolated from the genus *Podocarpus*, and some have been documented to possess various biological activities, such as antifungal, anti-inflammatory, and antiatherosclerotic activities [3–5]. Previously, we reported that nagilactone E (NLE), a dinorditerpenoid isolated from the seeds of *Podocarpus nagi*, exhibits anticancer activity in lung cancer in vitro. NLE treatment inhibited the proliferation of lung cancer cells via G2 phase cell cycle arrest mediated by the downregulation of Cyclin B1 [6]. In addition, NLE inhibited TGF-β1-induced epithelial–mesenchymal transition (EMT), migration and invasion in A549 cells via inhibition of the TGF-β-Smad2/3 signaling pathway [7]. However, the anticancer effects of NLE have not been studied in vivo, and the precise mechanisms of NLE remain to be further clarified.

Investigations of the mechanisms of natural products are generally difficult due to their diverse biological activities and multiple targets. Rapidly developed modern systematic methods, including network pharmacology and sequencing technologies, light the way for mechanistic studies and the further development of natural products [8, 9]. In recent years, a series of massively parallel "next generation" sequencing technologies have been well developed and dramatically changed the landscape of the genetic, biological, and medical sciences [10, 11]. RNA sequencing (RNA-seq) analysis is a mature and powerful sequencing-based approach for the characterization and quantification of transcriptomes [12]. It enables researchers to obtain precise and comprehensive information on absolute transcript expression levels within a single experiment. RNA-seq together with systematic bioinformatic analysis have been increasingly used for various applications, including investigations of the mechanisms of drug action and gene function [13, 14].

In this study, the in vivo anticancer effects of NLE were studied in a mouse xenograft model. Human lung cancer A549 cells treated with NLE were subjected to RNA-seq and bioinformatic analyses. NLE was shown to inhibit protein synthesis, and the inhibitory effect of NLE on de novo protein synthesis in A549 cells was further confirmed using the Click-iT assay.

MATERIALS AND METHODS

Reagents

NLE with a purity of approximately 99.99% was isolated from the seeds of *P. nagi* as documented in a previous study [6]. Cycloheximide; anti-rabbit IgG; anti-mouse IgG; and primary antibodies against NRF2, p21, STAT3, ATF4 and GAPDH were obtained from Cell Signaling Technology (Beverly, MA, USA).

[1]State Key Laboratory of Quality Research in Chinese Medicine, Institute of Chinese Medical Sciences, University of Macau, Macao, China; [2]School of Medicine, Chengdu University, Chengdu 610106, China; [3]Hubei Key Laboratory of Natural Medicinal Chemistry and Resource Evaluation, School of Pharmacy, Tongji Medical College, Huazhong University of Science and Technology, Wuhan 430074, China and [4]College of Pharmacy and Bioengineering, Chongqing University of Technology, Chongqing 401331, China
Correspondence: Li-gen Lin (LigenL@um.edu.mo) or Hua Li (li_hua@hust.edu.cn) or Jin-jian Lu (jinjianlu@um.edu.mo)

Received: 13 August 2019 Accepted: 8 November 2019
Published online: 11 February 2020

Primary antibody against β-actin was purchased from Santa Cruz Biotechnology (Dallas, CA, USA). RIPA lysis buffer was procured from Beyotime Biotechnology (Shanghai, China). Cisplatin was purchased from Selleck Chemicals (Houston, TX, USA). The reagents used for the Click-iT assay, Click-iT™ AHA (L-azidohomoalanine), biotin alkyne (PEG4 carboxamide-propargyl biotin), a Click-iT™ protein reaction buffer kit, and anti-streptavidin-HRP, were purchased from Life Technologies (Eugene, OR, USA). The bicistronic reporter plasmid pcDNA3-RLUC-POLIRES-FLUC constructed by Nahum Sonenberg was obtained from Addgene (plasmid # 45642) [15].

Cell culture
Human A549 lung cancer cells were acquired from the American Type Culture Collection (ATCC, Rockville, MD, USA). A549 cells were cultured in RPMI-1640 medium containing 10% fetal bovine serum and 1% penicillin–streptomycin (Gibco, Thermo Fisher Scientific, Carlsbad, CA, USA).

Mouse xenograft model
The in vivo assays were performed at Tongji Medical College, Huazhong University of Science and Technology. All of the animal experiments were approved by the Laboratory Animal Center of Huazhong University of Science and Technology and the Ethics Committee. CB-17/SCID mice (male, weight 14–16 g) were provided by Beijing Vital River Laboratory Animal Technology Co., Ltd (Beijing, China). Human lung cancer A549 cells (4×10^7 cells) were used to subcutaneously inoculate the right armpit of each mouse. Seven days later, the mice were randomly divided into different groups and intraperitoneally administered one of the following treatments daily for 3 weeks: (1) vehicle control group ($n = 8$), (2) 10 mg/kg/d NLE treatment group ($n = 8$). The NLE dose was selected according to the results of preliminary experiments. NLE was dissolved in a solution of polyoxyethylene castor oil:ethanol (1:1, v/v) at a concentration of 50 mg/mL and sonicated for 30 min to promote dissolution of the compound, which was diluted with physiological saline immediately before use. Cisplatin was administered at 2.5 mg/kg every other day as a positive control. Tumor sizes were measured with Vernier calipers, and tumor volumes were calculated with the following formula: $A \times B^2 \times \pi/6$, where A is the length and B is the width. The weights of the mice were recorded every other day. After the mice were sacrificed, tumor weight was measured. Hematoxylin-eosin (H&E) staining was applied to analyze pathological changes in the liver, spleen and kidney.

RNA-seq analysis
Exponentially growing A549 cells were trypsinized, resuspended, seeded into six-well plates and cultured for 24 h. The cells were treated with 0 or 4 μM NLE for another 24 h. Then, total RNA was extracted from the cells by using TRIzol reagent (Life Technologies, Shanghai, China). Quality control (QC) of the RNA samples was carried out using agarose gel electrophoresis and an Agilent 2100 Bioanalyzer. cDNA libraries were constructed from the RNA samples using the Illumina TruSeq mRNA library kit, and 2×150 paired-end RNA-seq was performed by WuXi AppTec (Shanghai, China) using an Illumina HiSeq X sequencing system.

Gene ontology (GO) and pathway enrichment analyses
Differentially expressed genes (DEGs) were subjected to GO and pathway enrichment analyses. Gene set enrichment analysis of GO terms and Kyoto Encyclopedia of Genes and Genomes (KEGG) pathway analysis were performed using the online DAVID 6.8 bioinformatics resources.

Quantitative real-time PCR assay
Total RNA was extracted from whole cells with TRIzol reagent, and cDNA was then synthesized by using a Transcriptor First Strand cDNA Synthesis Kit (Roche, Germany). qPCR was carried out using a SYBR Green kit (Roche, Germany), and results were detected by using the Mx3005P quantitative PCR system (Agilent Technologies, USA). The primers used are listed in Table 1.

Western blotting analysis
Western blotting analysis was performed to determine the expression levels of the proteins as documented in a previous study [16].

Click-iT assay
Exponentially growing A549 cells were trypsinized, resuspended, seeded into six-well plates and grown to approximately 80% confluence. Then, the cells were pretreated with NLE, CHX, or CIS for 30 min. After treatment, the medium was removed, and the cells were washed three times with PBS. Then, methionine-free RPMI-1640 medium (with NLE/CHX/CIS) was added and incubated for another 30 min. Then, the labeling compound AHA was added to the medium at a final concentration of 40 μM and incubated for 2 h. After washing three times with PBS, cell lysates were harvested by the addition of lysis buffer (1% sodium dodecyl sulfate in 50 mM Tris-HCl, pH 8.0). After centrifugation, the protein contents of the cell lysates were detected using a BCA™ protein assay kit. Click reactions were carried out by using 100 μg of cell lysate, biotin alkyne, and a Click-iT™ protein reaction buffer kit according to the manufacturer's instructions. Thereafter, the biotinylated proteins were purified via methanol/chloroform extraction and subjected to Western blotting. Membranes were probed with anti-streptavidin-HRP antibody. The unprocessed lysates were also subjected to Western blotting analysis and probed for β-actin. Protein expression was detected using ECL Select Western blot detection reagent (GE Healthcare, Buckinghamshire, UK).

Luciferase assay
Exponentially growing A549 cells were transfected with pcDNA3-RLUC-POLIRES-FLUC plasmid using TurboFect transfection reagent (Thermo Scientific, Lithuania). After transfection for 24 h, the cells were trypsinized, seeded in 12-well plates, incubated overnight, and further treated with NLE or CHX for 6 h. Luciferase activity was measured using a dual-luciferase reporter assay system (Promega, Madison, WI, USA) in accordance with the manufacturer's instructions.

Table 1. The primers used for quantitative real-time PCR.

Gene	Forward (5′–3′)	Reverse (5′–3′)
NRF2	ACACGGTCCACAGCTCATC	TGTCAATCAAATCCATGTCCTG
p21	CTGCCCAAGCTCTACCTTCC	CAGGTCCACATGGTCTTCCT
STAT3	TGACATTCCCAAGGAGGAGGC	TGCAGCTTCCGTTCTCAGCTCC
ATF4	AGATGACCTGGAAACCATGC	AGGGATCATGGCAACGTAAG
GAPDH	GCGACACCCACTCCTCCACCTTT	TGCTGTAGCCAAATTCGTTGTCATA

Molecular docking

The crystal structure of the human RIOK2 kinase domain (PDB code: 6HK6) was obtained from the Protein Data Bank (http://www.rcsb.org). Molecular docking was performed using ICM-Pro 3.8.2 modeling software on an Intel i7 4960 processor (MolSoft LLC, San Diego, CA) [17]. The ligand-binding pocket was selected with graphical tools in the ICM software to create the boundaries for the docking search. The chemical structure of the compound was input with mol2 files for docking. In the docking calculation, default parameters were applied to calculate the potential energy maps of the receptor. The compound was imported into the ICM and filed as an index project. Conformational sampling was based on the Monte Carlo procedure, and finally, the ligand with the lowest energy and most favorable orientation was selected.

Statistical analysis

Data are displayed as the mean ± standard deviation. Statistical analyses were conducted by using one-way analysis of variance with GraphPad Prism 6 (GraphPad Software, Inc., CA, USA). $P < 0.05$ and $P < 0.01$ indicated statistically significant differences.

RESULTS

NLE suppressed tumor growth in vivo

An A549 cell lung cancer xenograft mouse model was constructed using CB-17/SCID mice to evaluate the anticancer efficacy of NLE in vivo. As shown in Fig. 1a, the intraperitoneal injection of 10 mg/kg/d NLE markedly suppressed the growth of the tumors. After 3 weeks of treatment, all of the mice in the NLE treatment group ($n = 8$) as well as the control group ($n = 8$) were alive. However, in the cisplatin treatment group, mouse body weight had decreased significantly, and cisplatin treatment was terminated since two mice in the cisplatin treatment group died after 16 days of treatment. Mice in the control and NLE treatment groups were then sacrificed, their tumors were photographed, and the average tumor weights were measured (Fig. 1b). The tumor weight of the control group was 0.21 ± 0.06 g, whereas that of the NLE-treated group was 0.08 ± 0.06 g, representing a significant reduction in weight by 61.9%. Compared with the body weights of mice in the control group, NLE treatment did not have an obvious effect on mouse body weight (Fig. 1c). Moreover, H&E staining indicated obvious pathological damage in the liver tissue sections of the model group, indicating lesion metastasis of A549 orthotopic tumor to the liver tissue (Fig. 1d). NLE treatment reversed tumor metastasis and ameliorated hepatic pathology. Overall, these results indicated that NLE could suppress tumor growth in vivo.

RNA-seq analysis of differentially expressed genes

To identify DEGs in A549 cells after NLE treatment, RNA-seq analysis was performed. Gene abundance estimation was carried out using RSEM software (v1.2.29) [18]. Tens of thousands of expressed genes were detected, and the R package edgeR (v3.8.5) was used to compare the expression levels between the sample pairs (NLE vs control groups) [19]. The criteria for DEG detection in this study were a fold change > 2 and false discovery rate < 0.05. A heatmap of the gene expression levels of all the samples is shown in Fig. 2a. A total of 1341 genes were specifically upregulated, and 1924 genes were specifically downregulated in A549 cells treated with NLE compared with control cells.

To better understand the potential biological processes associated with the effects of NLE in lung cancer A549 cells, GO analysis was performed using the online DAVID 6.8 bioinformatics resource. Among "biological process" (BP) terms, the upregulated genes were mainly enriched in the regulation of transcription, rRNA processing and ribosome biogenesis terms, while the downregulated genes were mainly enriched in the oxidation-reduction, cholesterol biosynthetic processes, and lipid metabolic process terms. With respect to "molecular function" (MF) terms, the upregulated genes were mainly enriched in terms related to binding (RNA, nucleic acid, protein, DNA, etc.), while the downregulated genes were mainly enriched in the calcium ion binding and oxidoreductase activity terms. The top 10 most significantly enriched BP and MF terms are listed in Fig. 2b, c, respectively.

Thereafter, KEGG pathway enrichment analysis of the DEGs was carried out. The top 10 most significantly enriched KEGG pathways in A549 cells after NLE treatment are listed in Fig. 2d. Among these significantly enriched pathways, ribosome biogenesis in eukaryotes appeared to be the most enriched pathway in the upregulated genes, while metabolic pathways appeared to be the most enriched pathways in the downregulated genes. In addition, other

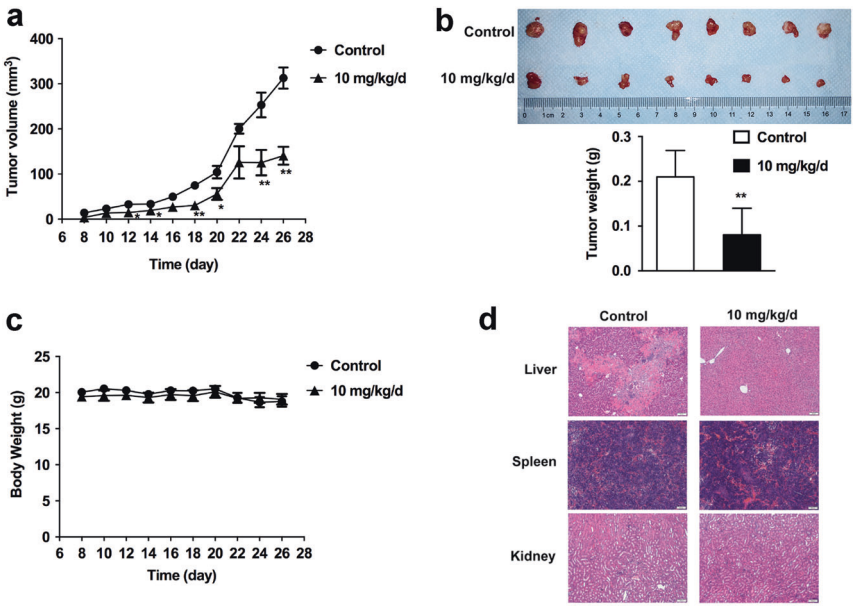

Fig. 1 NLE suppressed tumor growth in a lung cancer xenograft mouse model. a The average tumor volume in control mice ($n = 8$) and NLE-treated mice ($n = 8$, 10 mg/kg/d, i.p.) ~4 weeks after A549 cell injection. **b** After treatment for 3 weeks, the mice were sacrificed, their tumors were photographed, and differences in tumor weight were determined. **c** Mouse body weights. **d** H&E staining of liver, spleen and kidney biopsy samples, 200 ×, bar = 50 μm. *$P < 0.05$, **$P < 0.01$, compared with the vehicle-treated control group.

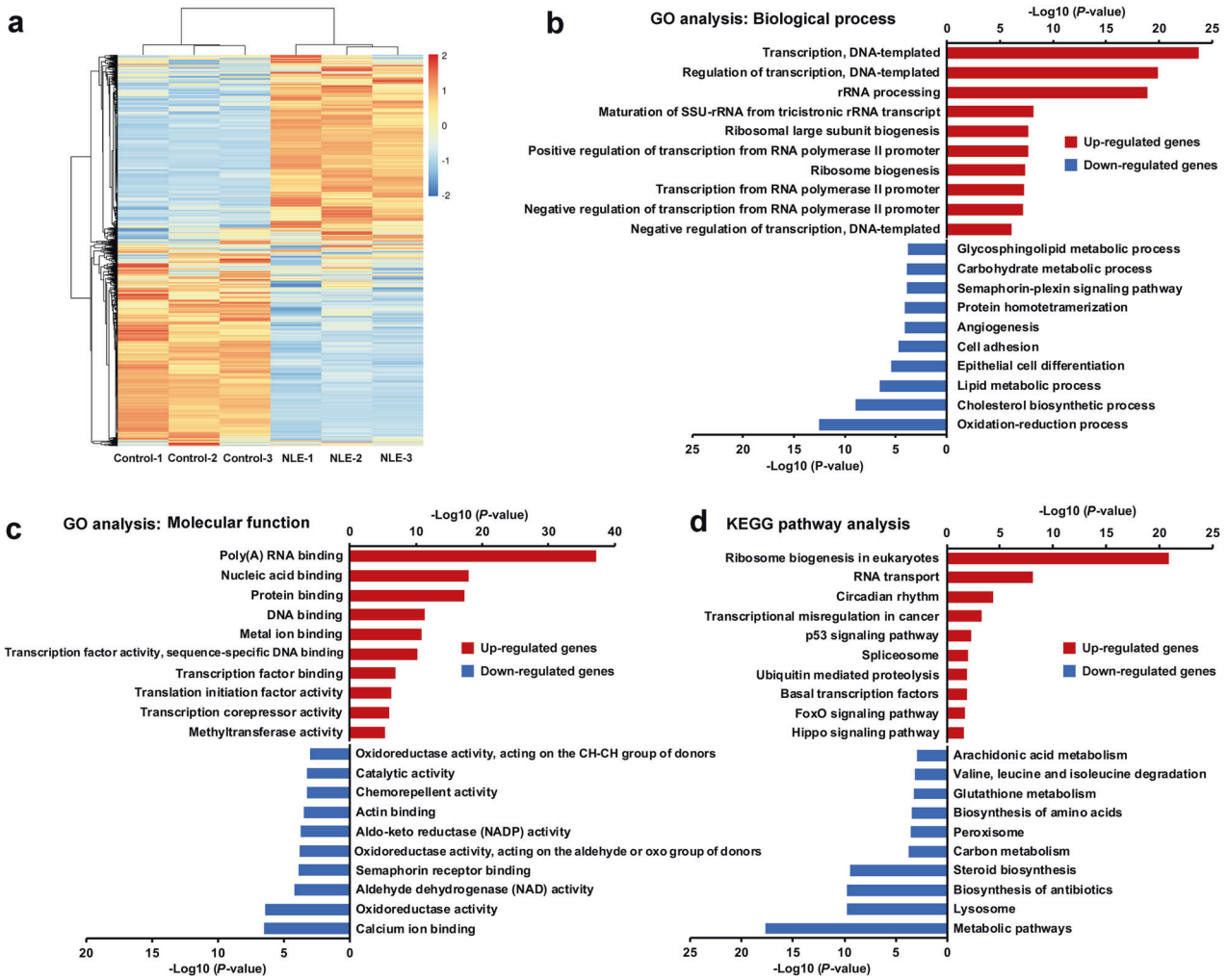

Fig. 2 RNA-seq analysis of differentially expressed genes after NLE treatment. a Heatmap showing RNA-seq data from A549 cells after NLE treatment. **b**, **c** Top 10 most significantly enriched GO terms in terms of "biological process" (BP) and "molecular function" (MF) in lung cancer A549 cells after NLE treatment. **d** Top 10 most significantly enriched KEGG pathways in lung cancer A549 cells after NLE treatment.

pathways (RNA transport, lysosome, circadian rhythm, biosynthesis of antibiotics and steroids) were enriched in the DEGs, indicating the multiple functions of NLE in lung cancer A549 cells.

Analysis of the RNA-seq data using the CMap dataset

The Connectivity Map (CMap) dataset (https://clue.io/cmap) is a powerful and convenient database that contains data on transcriptional responses to chemical, genetic and disease perturbation in multiple cell lines [20–22]. The CMap dataset can help characterize new chemical entities as well as understand their potential molecular mechanisms by using gene expression signatures derived from treatment with a small molecule. To clarify the mechanisms underlying the anticancer effect of NLE in A549 lung cancer cells, we further analyzed the DEGs using the CMap dataset. Briefly, the top 150 most upregulated genes ($P < 0.01$) and top 150 most downregulated genes ($P < 0.01$) were subjected to CMap database analysis to discover compounds with similar effects on gene expression.

Among the results obtained from CMap analysis, the "median score" referred to the connectivity score, which was used to rank the similarity between instances in the database with NLE. Those at the top of the ranking with higher scores were more similar to NLE (the redder the color, the higher the degree of similarity) based on their gene expression signatures. Surprisingly, the highest connectivity score among perturbational classes was assigned to protein synthesis inhibitors (99.71) (Fig. 3a). Specifically, the highest connectivity score was assigned to emetine (99.89) (a protein synthesis inhibitor) (Fig. 3b). In addition, the following three protein synthesis inhibitors were given relatively high scores of 99.72, 99.72, and 99.69: cephaeline, homoharringtonine, and cycloheximide, respectively (Fig. 3b). In total, the NLE gene expression signatures were most similar to those of protein synthesis inhibitors, indicating that NLE is a potential protein synthesis inhibitor.

NLE inhibited the expression of short-lived proteins

Since short-lived proteins exhibit a short half-life, their expression levels might decrease rapidly upon the inhibition of de novo protein synthesis. RNA-seq analysis revealed a large number of genes that were upregulated after NLE treatment. Herein, the short-lived proteins NRF2, p21, STAT3 and ATF4 were selected for further verification to confirm their upregulated expression, as shown by RNA-seq. Briefly, A549 cells were treated with NLE (2, 4, and 8 μM) for 6 or 12 h, and then the mRNA and protein levels of NRF2, p21, STAT3, and ATF4 were determined by qPCR and Western blot analyses, respectively. As shown in Fig. 4a, the mRNA levels of NRF2, p21, STAT3, and ATF4 were upregulated after NLE treatment, which was consistent with the results obtained by RNA-seq analysis. In contrast, the protein levels of NRF2, p21, STAT3, and ATF4 were obviously decreased after NLE treatment (Fig. 4b), indicating that NLE might inhibit de novo synthesis of these proteins.

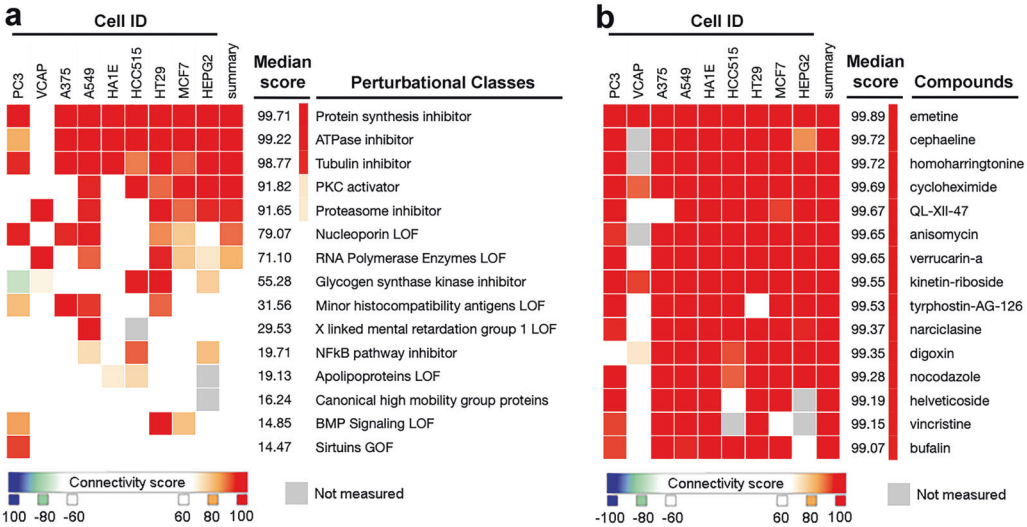

Fig. 3 CMap dataset analysis of RNA-seq data suggested that NLE is a protein synthesis inhibitor. The top 150 most upregulated genes ($P < 0.01$) and top 150 most downregulated genes ($P < 0.01$) were recruited and analyzed using the CMap database to compare them with differentially expressed genes classified by perturbational class (**a**) and compound (**b**).

The Click-iT assay confirmed NLE as a protein synthesis inhibitor

To confirm the results obtained by CMap dataset analysis as well as the inhibitory effect of NLE on the expression of short-lived proteins, the inhibitory effect of NLE on de novo protein synthesis in lung cancer A549 cells was further assessed by using the Click-iT assay. For the Click-iT assay, methionine-free medium was utilized for cell pretreatment and drug treatment; thus, newly synthesized proteins would be tagged with the labeling compound AHA, an amino acid analog of methionine containing an azido moiety, since methionine is the amino acid universally used to initiate new protein synthesis [23, 24]. Thereafter, biotinylation was carried out by using a copper-catalyzed "click" alkyne reaction, and biotin was subsequently detected with HRP-coupled streptavidin.

Herein, CHX and CIS were used as positive and negative controls, respectively. As shown in Fig. 5a, compared with the control group, treatment with the methionine analog AHA for 1 h followed by biotinylation allowed the remarkable visualization of newly synthesized proteins with Ultra Streptavidin-HRP antibody. CIS pretreatment had no effect on the visualization of newly synthesized proteins, while pretreatment with the well-known protein synthesis inhibitor CHX (50 μM) completely abolished de novo protein synthesis. In addition, pretreatment with 2 μM NLE partially inhibited de novo protein synthesis, while 4 μM NLE pretreatment completely abolished de novo protein synthesis in A549 cells.

NLE inhibited both cap-dependent and cap-independent translation

The dual pcDNA3-RLUC-POLIRES-FLUC reporter luciferase assay was performed to evaluate the effects of NLE on cap-dependent and cap-independent translation. In the pcDNA3-RLUC-POLIRES-FLUC plasmid, the RLUC cistron undergoes cap-dependent translation, while the FLUC cistron undergoes cap-independent translation as it is directed by the poliovirus IRES [15]. As shown in Fig. 5b, NLE (2 and 4 μM) significantly inhibited the fluorescence intensity of both firefly and Renilla luciferase as well as positive control cells treated with CHX (50 μM), indicating that NLE inhibited both cap-dependent and cap-independent translation in A549 cells.

Molecular docking identified low-energy binding conformations of NLE bound to RIOK2

To discover the targets of NLE, molecular docking was carried out. Several proteins have been identified as potential targets of NLE, among which RIOK2 exhibited the highest binding affinity with NLE; therefore, the inhibitory effect of NLE on RIOK2 was elucidated. Molecular docking was performed with ICM-Pro 3.8.2 modeling software (MolSoft LLC, San Diego, CA) [17] with the crystal structure of the RIOK2 kinase domain as the template (PDB code: 6HK6) [25]. NLE at the lowest-energy binding conformation is shown in Fig. 6a. As seen from the generated docking model, NLE fit well into a relatively shallow pocket formed between the winged helix-turn-helix (wHTH) domain and N-terminal lobe (N-lobe) of RIOK2. The binding of NLE in this allosteric site was suggested to lock the kinase in an inactive conformation, thus inhibiting its activity. This binding pocket was relatively hydrophobic, and hydrophobic interactions were predicted between Phe17 and ring A, Tyr11 and ring C, and Ser90 and ring B. In addition, several hydrogen-binding interactions between Arg14 with the carbonyl group of ring D and Met12 and Lys86 with the carbonyl group of ring C were predicted (Fig. 6b).

DISCUSSION

We previously reported the inhibitory effects of NLE on the proliferation, TGF-β1-induced EMT, migration and invasion of lung cancer cells in vitro [6, 7]. The in vivo study herein further confirmed that the intraperitoneal injection of 10 mg/kg/d NLE suppressed tumor growth in a xenograft model without obvious toxicity. Moreover, NLE treatment also inhibited tumor metastasis, as evidenced by H&E staining. Thus, NLE has been demonstrated to be an effective anticancer candidate both in vitro and in vivo. However, during this study, we also found that NLE showed relatively poor solubility in solvent, which might somehow have affected the efficacy of NLE in this in vivo study. Thus, in future work, structural modification based on analysis of the structure-activity relationship or pharmaceutical approaches, such as nanoparticle technology and micelle preparation, should be taken into consideration to further improve the solubility and drug-like properties of NLE [26].

To further clarify the mechanisms of NLE, RNA-seq and bioinformatic analyses were carried out. In particular, as evidenced by CMap dataset analysis, a number of substances and proteins were determined to produce gene expression signatures markedly similar to that following NLE treatment. Emetine is an FDA-approved compound for amebiasis that has been documented for decades as a protein synthesis inhibitor via its binding to the 40 S

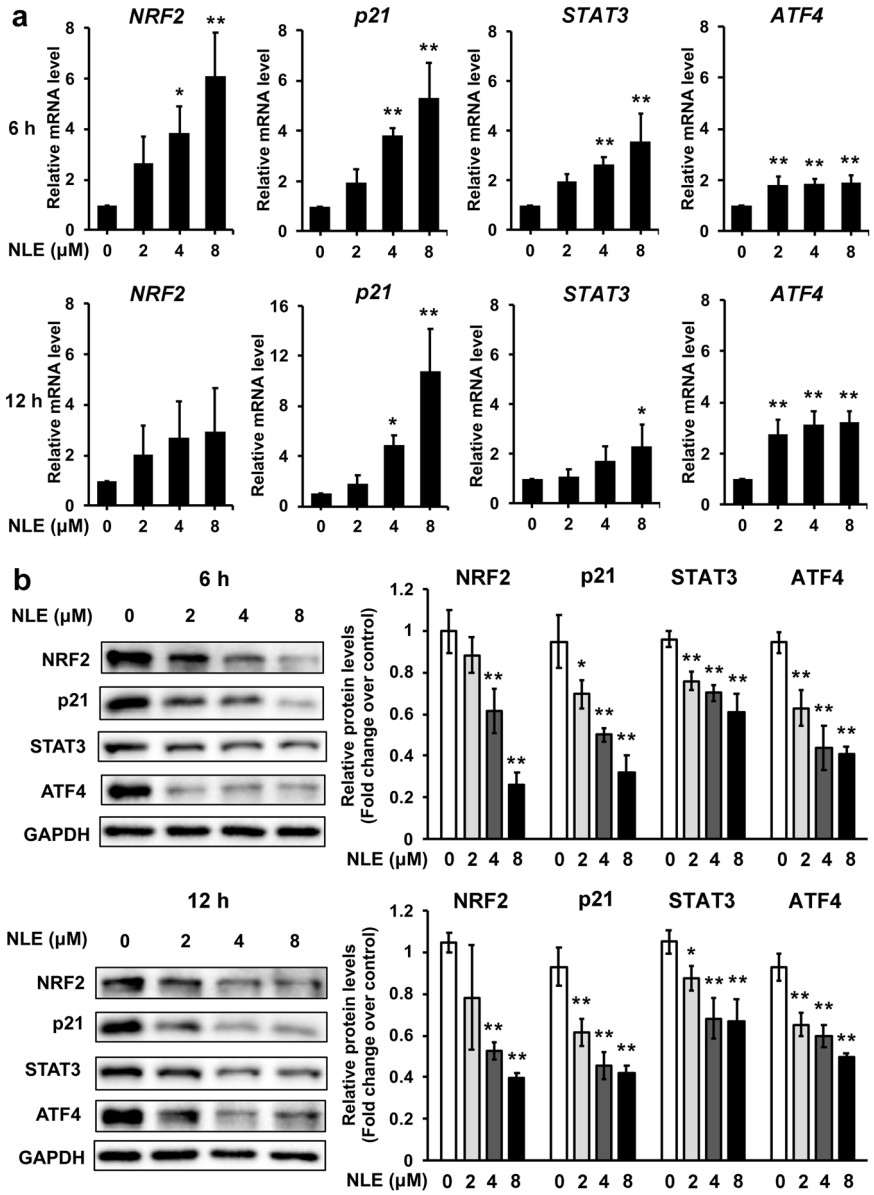

Fig. 4 NLE inhibited the expression of short-lived proteins. A549 cells were treated with NLE for 6 or 12 h. **a** The mRNA levels of *NRF2*, *p21*, *STAT3*, and *ATF4* were determined by qPCR assay. **b** The protein levels of NRF2, p21, STAT3, and ATF4 were detected by Western blot analysis. $^{*}P < 0.05$, $^{**}P < 0.01$, compared with the control group.

subunit of the ribosome [27, 28]. Meanwhile, very high connectivity scores (scores > 99.5) were also awarded to a class of well-known protein synthesis inhibitors, such as cephaeline, the structural desmethyl analog of cephaeline [29]; homoharringtonine; and the most commonly used protein synthesis inhibitor cycloheximide [30]. Thereafter, the inhibitory effect of NLE on de novo protein synthesis in A549 cells was further confirmed using the Click-iT assay. CHX is a both cap-dependent and cap-independent protein synthesis inhibitor [31]. We further performed a luciferase assay with the reporter plasmid pcDNA3-RLUC-POLIRES-FLUC and found that NLE and CHX inhibited both cap-dependent and cap-independent translation. The results of our previous study indicated that NLE might inhibit the translation of Cyclin B1 since it decreased Cyclin B1 protein levels without inhibiting the transcription or promoting the degradation of Cyclin B1 [6]. Moreover, in our study on the inhibitory effects of NLE on TGF-β1-induced EMT in NSCLC cells, we found that NLE treatment inhibited the expression of TβRI and a series of mesenchymal and invasiveness markers, and we also deduced that de novo protein synthesis inhibition might partially contribute to the inhibitory effects of NLE on some regulators responsible for the TGF-β1-induced upregulation of TβRI [6]. The results obtained here are also consistent with our previous hypothesis.

Previously, by comparing cytotoxicity profiles, nagilactone C, an analog of NLE, was reported to be a translation inhibitor [32]. Nagilactone C inhibited the elongation of protein synthesis without preventing ribosome binding to mRNA templates. Nagilactone C treatment inhibited the eEF-1α-dependent binding of aminoacyl-tRNA to the ribosomal A site, as well as peptidyl transferase activity [32]. NLE was also demonstrated to be a protein synthesis inhibitor in our study. Moreover, the precise effects of NLE on absolute transcript expression levels were clarified by using RNA-seq. Systematic bioinformatic analysis through GO (BP and MF terms) and KEGG pathway analysis has provided comprehensive gene expression signatures following treatment with NLE and can help us better understand the

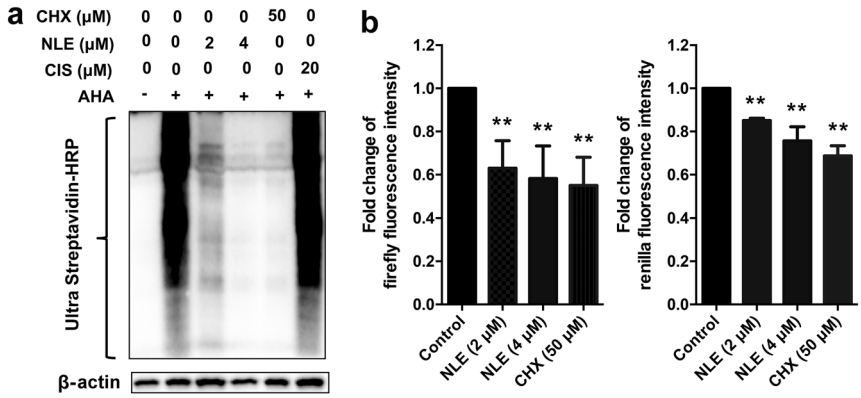

Fig. 5 NLE inhibited both cap-dependent and cap-independent de novo protein synthesis. a A549 cells were pretreated with NLE, CHX, or CIS at the indicated concentration for 30 min, then washed three times with PBS and further cultured in methionine-free RPMI 1640 medium (with NLE/CHX/CIS) for another 30 min. Then, the labeling compound AHA was added to the medium at a final concentration of 40 μM for 2 h of treatment. AHA was withheld from a control well to assess the background signal. After washing three times with PBS, cell lysates were harvested, and Click reactions were performed using 100 μg of cell lysate, biotin alkyne, and a Click-iT™ protein reaction buffer kit. The biotinylated proteins were purified and subjected to Western blotting. **b** A549 cells were transfected with the pcDNA3-RLUC-POLIRES-FLUC plasmid. After transfection for 24 h, the cells were trypsinized, seeded in 12-well plates, incubated overnight, and further treated with NLE or CHX for 6 h. Luciferase activity was measured using the dual-luciferase reporter assay system.

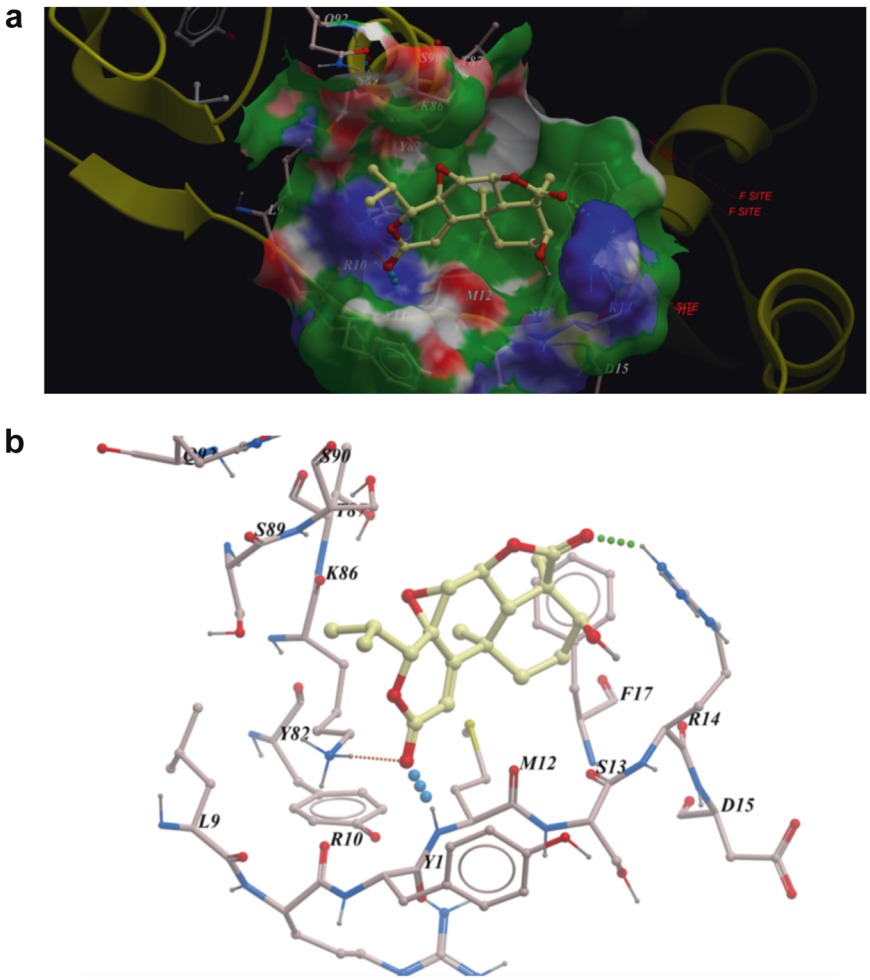

Fig. 6 Low-energy binding conformations of NLE bound to RIOK2 generated by molecular docking. a NLE bound to an allosteric pocket formed between the wHTH domain and N-lobe of RIOK2. **b** Detailed view of NLE binding to the allosteric site of the enzyme. Residues in RIOK2 and NLE are depicted in a ball and stick model showing carbon (yellow), oxygen (red), nitrogen (blue), and hydrogen (gray) atoms. Hydrogen bonds are represented by dotted lines.

biological activities and mechanisms of NLE. According to the results, more than one thousand genes were specifically upregulated after NLE treatment. In our opinion, some of these genes might be upregulated via a feedback mechanism. Moreover, NLE might promote the expression of a number of genes, as it is a natural compound with multiple targets. Molecular docking was carried out for target prediction, and NLE exhibited an outstanding binding affinity with RIOK2. RIOK2 belongs to an evolutionarily conserved family of atypical kinases that are related to the ribosome maturation process [25]. A recent study indicated that the expression level of RIOK2 can predict clinical outcome in NSCLC and might serve as a target for NSCLC therapy [33]. Moreover, we then performed Kaplan–Meier analysis of RIOK2 expression and overall survival in some other cancer types. Kaplan–Meier survival curves indicated that high RIOK2 expression was correlated with poorer overall survival compared with low RIOK2 expression in patients with liver hepatocellular carcinoma, kidney renal papillary cell carcinoma, head and neck squamous cell carcinoma, and bladder carcinoma (Fig. S1). Based on these results, we deduce that RIOK2 is a potential target of NLE, which should be further confirmed by surface plasmon resonance, isothermal titration calorimetry, or other techniques in future work.

In summary, NLE was demonstrated to suppress tumor growth in a xenograft model without obvious toxicity. RNA-seq analysis was carried out to further investigate the underlying mechanisms of NLE. The effects of NLE on A549 cells were illustrated by GO and pathway enrichment analyses. CMap dataset analysis supported NLE as a protein synthesis inhibitor, which was further confirmed by the Click-iT assay. Molecular docking predicted RIOK2 as a target of NLE. Taken together, the results of our study demonstrated that NLE is a protein synthesis inhibitor.

ACKNOWLEDGEMENTS

This work was supported by the Science and Technology Development Fund, Macau SAR (File no. 176/2017/A3), and the Research Fund of the University of Macau (MYRG2018-00165-ICMS, CPG2019-00006-ICMS, and MYRG2015-00153-ICMS-QRCM). We thank Prof. Yun Tang (East China University of Science and Technology) for his kindly help with this work.

AUTHOR CONTRIBUTIONS

LLZ and JJL designed this study. LGL provided the compound NLE. LLZ and JG performed the experiments. LLZ, HL and JJL drafted the paper. LLZ, XMJ, HL and JJL analyzed the data. All the authors participated in the revision and improvement of the paper.

ADDITIONAL INFORMATION

The online version of this article (https://doi.org/10.1038/s41401-019-0332-7) contains supplementary material, which is available to authorized users.

Competing interests: The authors declare no competing interests.

REFERENCES

1. Feng ZL, Zhang LL, Zheng YD, Liu QY, Liu JX, Feng L, et al. Norditerpenoids and dinorditerpenoids from the seeds of *Podocarpus nagi* as cytotoxic agents and autophagy inducers. J Nat Prod. 2017;80:2110–7.
2. Addo EM, Chai H-B, Hymete A, Yeshak MY, Slebodnick C, Kingston DG, et al. Antiproliferative constituents of the roots of Ethiopian Podocarpus falcatus and structure revision of 2α-hydroxynagilactone F and nagilactone I. J Nat Prod. 2015;78:827–35.
3. Hayashi K, Yamaguchi Y, Ogita A, Tanaka T, Kubo I, Fujita KI. Effect of nagilactone E on cell morphology and glucan biosynthesis in budding yeast *Saccharomyces cerevisiae*. Fitoterapia. 2018;128:112–7.
4. Feng ZL, Zhang T, Liu JX, Chen XP, Gan LS, Ye Y, et al. New podolactones from the seeds of *Podocarpus nagi* and their anti-inflammatory effect. J Nat Med. 2018;72:882–9.
5. Gui Y, Yao S, Yan H, Hu L, Yu C, Gao F, et al. A novel small molecule liver X receptor transcriptional regulator, nagilactone B, suppresses atherosclerosis in apoE-deficient mice. Cardiovasc Res. 2016;112:502–14.
6. Zhang LL, Feng ZL, Su MX, Jiang XM, Chen X, Wang Y, et al. Downregulation of Cyclin B1 mediates nagilactone E-induced G2 phase cell cycle arrest in non-small cell lung cancer cells. Eur J Pharmacol. 2018;830:17–25.
7. Zhang LL, Jiang XM, Huang MY, Feng ZL, Chen X, Wang Y, et al. Nagilactone E suppresses TGF-β1-induced epithelial–mesenchymal transition, migration and invasion in non-small cell lung cancer cells. Phytomedicine. 2019;52:32–9.
8. Luo F, Gu J, Chen L, Xu X. Systems pharmacology strategies for anticancer drug discovery based on natural products. Mol Biosyst. 2014;10:1912–7.
9. Schenone M, Dančík V, Wagner BK, Clemons PA. Target identification and mechanism of action in chemical biology and drug discovery. Nat Chem Biol. 2013;9:232.
10. Van Dijk EL, Auger H, Jaszczyszyn Y, Thermes C. Ten years of next-generation sequencing technology. Trends Genet. 2014;30:418–26.
11. Buermans H, Den Dunnen J. Next generation sequencing technology: advances and applications. BBA-Mol Basis Dis. 2014;1842:1932–41.
12. Costa V, Angelini C, De Feis I, Ciccodicola A. Uncovering the complexity of transcriptomes with RNA-Seq. BioMed Res Int. 2010;2010:853916.
13. Wacker SA, Houghtaling BR, Elemento O, Kapoor TM. Using transcriptome sequencing to identify mechanisms of drug action and resistance. Nat Chem Biol. 2012;8:235.
14. Zhang W, Bouchard G, Yu A, Shafiq M, Jamali M, Shrager JB, et al. GFPT2-expressing cancer-associated fibroblasts mediate metabolic reprogramming in human lung adenocarcinoma. Cancer Res. 2018;78:3445–57.
15. Poulin F, Gingras AC, Olsen H, Chevalier S, Sonenberg N. 4E-BP3, a new member of the eukaryotic initiation factor 4E-binding protein family. J Biol Chem. 1998;273:14002–7.
16. Zhang LL, Xu YL, Tang ZH, Xu XH, Chen X, Li T, et al. Effects of alisol B 23-acetate on ovarian cancer cells: G1 phase cell cycle arrest, apoptosis, migration and invasion inhibition. Phytomedicine. 2016;23:800–9.
17. Abagyan R, Totrov M, Kuznetsov D. ICM—a new method for protein modeling and design: applications to docking and structure prediction from the distorted native conformation. J Comput Chem. 1994;15:488–506.
18. Robinson MD, McCarthy DJ, Smyth GK. edgeR: a Bioconductor package for differential expression analysis of digital gene expression data. Bioinformatics. 2010;26:139–40.
19. Anders S, Huber W. Differential expression analysis for sequence count data. Genome Biol. 2010;11:R106.
20. Lamb J, Crawford ED, Peck D, Modell JW, Blat IC, Wrobel MJ, et al. The Connectivity Map: using gene-expression signatures to connect small molecules, genes, and disease. Science 2006;313:1929–35.
21. Michnick SW. The connectivity map. Nat Chem Biol. 2006;2:663.
22. Lamb J. The Connectivity Map: a new tool for biomedical research. Nat Rev Cancer. 2007;7:54–60.
23. Vartanian S, Ma TP, Lee J, Haverty PM, Kirkpatrick DS, Yu K, et al. Application of mass spectrometry profiling to establish brusatol as an inhibitor of global protein synthesis. Mol Cell Proteom. 2016;15:1220–31.
24. Song W, Wang Y, Yu Z, Vera CIR, Qu J, Lin Q. A metabolic alkene reporter for spatiotemporally controlled imaging of newly synthesized proteins in mammalian cells. ACS Chem Biol. 2010;5:875–85.
25. Wang J, Varin T, Vieth M, Elkins JM. Crystal structure of human RIOK2 bound to a specific inhibitor. Open Biol. 2019;9:190037.
26. Huang MY, Zhang LL, Ding J, Lu JJ. Anticancer drug discovery from Chinese medicinal herbs. Chin Med. 2018;13:35.
27. Jimenez A, Carrasco L, Vazquez D. Enzymic and nonenzymic translocation by yeast polysomes. Site of action of a number of inhibitors. Biochemistry. 1977;16:4727–30.
28. Gupta RS, Siminovitch L. The molecular basis of emetine resistance in Chinese hamster ovary cells: alteration in the 40S ribosomal subunit. Cell. 1977;10:61–6.
29. Yang S, Xu M, Lee EM, Gorshkov K, Shiryaev SA, He S, et al. Emetine inhibits Zika and Ebola virus infections through two molecular mechanisms: inhibiting viral replication and decreasing viral entry. Cell Discov. 2018;4:31. https://doi.org/10.1038/s41421-018-0034-1.
30. Ennis H, Lubin M. Cycloheximide: aspects of inhibition of protein synthesis in mammalian cells. Science. 1964;146:1474–6.
31. Harder B, Tian W, La Clair JJ, Tan AC, Ooi A, Chapman E, et al. Brusatol overcomes chemoresistance through inhibition of protein translation. Mol Carcinog. 2017;56:1493–500.
32. Chan J, Khan SN, Harvey I, Merrick W, Pelletier J. Eukaryotic protein synthesis inhibitors identified by comparison of cytotoxicity profiles. RNA. 2004;10:528–43.
33. Liu K, Chen HL, Wang S, Gu MM, Chen XM, Zhang SL, et al. High expression of RIOK2 and NOB1 predict human non-small cell lung cancer outcomes. Sci Rep. 2016;6:28666. https://doi.org/10.1038/srep28666.